AIChE

Separation of Dyes Using Composite Carbon Membranes

Sonny Sachdeva and Anil Kumar
Dept. of Chemical Engineering, Indian Institute of Technology Kanpur, Kanpur, UP 208016, India

DOI 10.1002/aic.11781
Published online May 28, 2009 in Wiley InterScience (www.interscience.wiley.com).

A composite, clay supported carbon membrane has been synthesized by carbonization of a blend of polyethylene glycol and phenol formaldehyde resin and the membrane thus obtained is characterized by separation of dyes. This membrane is subjected to permeability test using pure water which is found to be considerably higher than that reported in literature. It is subsequently shown to reject Acid Orange 7 dye from water with the rejection dependent on pressure and concentration of the dye which is typical phenomenon observed for a charged membrane. The separation data has been analyzed using the Space charge model and the membrane charge is estimated by minimizing the root mean square error between the experimental results and those calculated from the model. © 2009 American Institute of Chemical Engineers *AIChE J,* 55: 1712–1722, 2009

Keywords: carbon membrane, anionic dye, nanoseparation, space charge model, charged membranes

Introduction

The development of the first porous inorganic membranes took place for the separation of uranium isotopes and these were used mainly for military and nuclear purposes.[1] These have been made from various materials like oxides of alumina, titania, and zirconia, glass (silica), metals, zeolite, and carbon and are more expensive than polymeric membranes. They possess advantages of stability at high temperature and wear resistance, well-defined stable pore structure and chemical inertness.[2] Moreover, inorganic membranes have much higher organic solvent stability than the polymeric ones as the latter have a tendency to either swell or dissolve in solvents, thus causing irreversible damage to their structure and eventually loss of separation capabilities. Carbon membranes have proved promising for gas separation as it is more feasible to form crack free membranes of carbon compared to zeolite and glass membranes.[3]

Fabrication of porous carbon membranes mainly involves six important steps (a) precursor selection (b) polymeric membrane preparation (c) pretreatment (d) pyrolysis/carbonization (e) post treatment, and (f) module construction.[3,4] Among these steps, the pyrolysis is the most important step because during this stage, the pore structure of the carbon membrane is formed which is responsible for its separation properties. Different precursors for making carbon membranes have been cellulose and its derivatives,[5,6] polyacrylonitrile,[7] phenol-formaldehyde resin,[8] poly furfuryl alcohol,[9] polyimide,[10] graphite,[11] coal,[12] pitch and plants.[13,14] Polymeric membranes are subjected to pretreatment (physical, chemical, and oxidative) before pyrolysis so as to ensure the stability of the polymer precursor and the preservation of its structure during pyrolysis.

Apart from gas separation, there lies a large potential for these membranes to be used for aqueous and solvent based applications also as these are temperature and chemical resistant. Only a few works have been reported[14,15–23] that have explored carbon membranes for microfiltration and ultrafiltration applications. The characteristics and application of carbon microfiltration membranes are mainly determined by the pore structure and therefore, it is very important to closely control it. A unique way of controlling the pore structure is by preparing the membrane using polymer blends, with one component as thermally labile polymer and

Correspondence concerning this article should be addressed to A. Kumar at anilk@iitk.ac.in

the second, a thermally stable polymer. The decomposition of the thermally labile polymer creates mesopores (2–50 nm), while the thermally stable polymer leads to the formation of micropores (<2 nm) during pyrolysis. The pyrolysis of the blended polymer precursors leads to the formation of porous structure since the thermally labile polymer is completely decomposed at a lower temperature than the thermally stable polymer.[16,17] The most commonly used thermally labile polymers are poly(ethylene glycol), poly(vinyl butyral) and poly(vinylpyrrolidone).[17]

Strano et al.[18] have presented a method for producing carbon ultrafiltration membranes using spray deposition and pyrolysis (stream of flowing N_2, heating at the rate of 5°C/min and held at 600°C for 2 h) of poly(furfuryl alcohol)/poly(ethylene glycol) mixtures on macroporous stainless steel supports. Polyethylene glycols of different molecular weights (1000, 2000, 3400, and 8000 Da) have been used as a noncarbonizing template molecule to control porosity of the carbon film. Permeation of a polydisperse dextran solution has been used to quantify the retention properties of the membranes as a function of template size. Although nanoporous membranes have been prepared that had dextran sieving curves comparable to conventional ultrafiltration membranes, the water permeability for the nanoporous carbon was less than 10 l/m^{2}h bar, which is an order of magnitude lower than that of commercial inorganic and polymeric ultrafiltration membranes. This low permeability was a direct result of the large thickness of the selective layer (up to 15 μm) produced by the multiple pyrolysis steps required to make an integral membrane.[18]

Shah et al.[19] have prepared carbon membranes using spin-coating of the blended polymer [poly(furfuryl alcohal)/poly (ethylene glycol) mixtures] and carried out protein (Bovine serum albumin, BSA) separation from these membranes. The performance of the membranes has been compared with commercially available 100 kDa polyethersulfone ufltrafiltration membranes. They have slip-casted the stainless steel supports by silica particles to block the macropores to reduce the defects of the supports. They were able to obtain a 4-fold increase (41 l/m^{2}h bar) in the membrane permeability by reducing the thickness (7 μm) of the membranes.

Pugazehanthi et al.[23] have prepared noninterpreting ultrafiltration carbon membranes having pore size of 4.8 nm [determined from molecular weight cutoff (MWCO) experiments], using a resole type phenolic resin, and functionalized them by two-stage modification. In the first stage, the membranes were nitrated using NO_x at 250°C and in the second, aminated using hydrazine hydrate at 60°C. On doing this, the pore size increased to 7.0 nm and 8.0 nm for the nitrated and aminated membrane. They have carried out experiments on the removal of Cr (VI) from its aqueous solution using the unmodified, nitrated and aminated membranes, respectively. The unmodified membrane gave a rejection of 96%, while nitrated gave 84% and aminated 88%. In this work, we report the synthesis of a carbon membrane having 1.8-nm-pore diameter and find it suitable for separation of anionic dye (Acid Orange 7). The pure water permeability obtained for the carbon membrane synthesized in this work is almost two orders of magnitude more than that reported in our earlier work.[23]

Dye separation from industrial effluents is one of the most important environmental concerns.[24] Wastewater from textile processing plants can be highly colored and difficult to be decolorized. Over 15% of the textile dyes are lost in wastewater stream during dyeing operation. Dyes have been classified according to their chemical structure and have been put in the category of anionic, cationic, or nonionic dyes. Dyes do not degrade fully and cause environmental pollution and thus the recovery of spent liquor in order to reuse the salts and water is one of the thrust areas in membrane separations. The most widely used methods for dye removal are chemical, physical and biological. The chemical methods include oxidative processes like using Fenton's reagent,[25] sodium hypochlorite,[26] ozonation[27] and photochemical methods.[28] Various physical treatments include membrane separation processes, adsorption (activated carbon, peat, wood chips, silica gel and fly ash and coal mixture), ion exchange, irradiation, and electrokinetic coagulation that have been reviewed recently.[29] The biological methods include decolorization by white-rot fungi[30] and many more microorganisms reviewed by Forgacs et al.[31] Azo dyes like Acid Orange 7, that have the chromophore of —N=N— unit in their molecular structure, are known to be largely nonbiodegradable in aerobic conditions and reduce to more hazardous intermediates in anaerobic conditions. Azo dyes are very difficult to be treated in environmental systems, because the sulfonic acid groups in their structure make them very water-soluble and polar.[32]

In this work, a composite nanoporous carbon membrane has been synthesized using blend polymers that consist of a thermally labile polymer (polyethylene glycol, 400 Da) and a thermally stable polymer (phenol/formaldehyde resole) requiring much lower temperature (500°C as opposed to 900°C reported in literature). This has been further characterized using Fourier transform infrared spectroscopy (FTIR), scanning electron microscopy (SEM), AFM, MWCO, and contact angle measurements. The carbon membrane reported in this work has a higher pure water flux and permeability (1.8 times) than the membranes reported in literature.[19] The real rejection has been calculated by including the concentration polarization effects and the effect of pressure and feed concentration on it has been determined. It has been shown that the real rejection is in the range of 90–100% (as typical of charged membranes) and is dependent on the concentration of the solution and the pressure gradient. The separation results have been analyzed using Space charge model[33,34] and the wall potential of 85–100 mV and pore size of 1.8 nm was found to give the experimental observed.

Experimental

Materials

Analytical grade phenol crystals (99.5%), formaldehyde (37–41%, w/v), xylene, polyethylene glycol (PEG), Acid Orange 7 dye, ethanol, toluene, sodium hydroxide pellets were procured from SD Fine Chemicals (Mumbai, India).

Composite Carbon Membrane Preparation. The preparation of composite carbon membrane constitutes three main steps. Firstly, the ceramic support is prepared from a mixture of clays. This is followed by the preparation of polymer precursor mixture of resole type phenol formaldehyde resin and

PEG in ethanol. Finally, the polymer solution is spin coated on the clay support, cross-linked by further heating and carbonized to get a porous carbon membrane. In the following sections, each of these steps is described in detail.

Preparation of Clay Supports. An integral part of the supported membranes is the support itself which provides mechanical and chemical strength to it. We have prepared clay supports using different clays (kaolin, ball clay, pyrophallite, calcium carbonate, feldspar, and quartz) following a procedure already reported in our previous work.[34] The materials are mixed well in the given composition with distilled water to obtain a homogeneous paste and then cast in the form of circular disc on a gypsum surface. The supports are first dried in a first at room temperature overnight, then at 100°C for about 24 h and finally at 250°C for another 24 h. After the complete drying of the supports, they are calcined at 900°C in the furnace for 12 h. These are further dipped in a solution of TEOS and calcined at 1000°C for a period of 5 h in a furnace.

Polymer Synthesis. The low molecular weight (300–700 g/mol) resole-type phenolic resin is prepared by condensation polymerization of phenol (94 g, 1 mol) and 37% aqueous formaldehyde (123 g, 1.5 mol) in presence of basic catalyst (sodium hydroxide, 5 g, 0.125 mol). The reaction mixture is refluxed in a 1 liter reactor at 95°C under continuous stirring for 5 h till a dark red colored viscous mass of the polymer is obtained. The polymer syrup, thus, prepared, is cooled immediately and stored at −5°C to arrest the polymerization reaction from progressing further. A mixture of PEG (molecular weight 400 g/mol) and phenol formaldehyde resin (PF) in 1:1 weight ratio is prepared in ethanol and stirred properly to make a homogeneous solution.

Preparation of Carbon Membrane. The polished clay support is dipped in xylene, a nonsolvent for the polymer solution, to displace the air present inside the pores. Since xylene is a volatile solvent, the clay support is kept on polyurethane foam completely soaked in xylene. Approximately, 2 g of a 60 wt % solution of polymer mixture (PF + PEG) in ethanol is spin-coated on the clay support (wet with xylene) at 1200 rpm. The polymer coated clay support is allowed to dry in air for 1 h at room temperature and then for 2 h at 60°C. The membrane is then cross-linked by heating it at 120°C for 12 h. A second coat of the polymer blend is applied on the membrane and again crosslinked at 120°C. The clay composite membrane is finally carbonized in N_2 atmosphere at a heating rate of 2.5–3°C/min and kept at 500°C for 1 h. After cooling the carbonized membrane to room temperature, it is flushed with water at high pressure to remove the gases adsorbed on its surface.

Characterization of Carbon Membrane

Fourier Transform Infrared Spectroscopy. The FTIR spectrum of the carbon membrane is obtained using Bruker VERTEX 22, Germany, spectrometer to identify the functional groups present on the membrane surface. Infrared spectra of fresh carbonized polymer films, crushed as powder samples, are obtained by making a pellet of 200 mg of IR spectroscopic grade KBr pellets and 1 mg of membrane sample in the range of 500–4000 cm^{-1}.

Scanning Electron Microscopy. The structural morphology of the surface and the cross-section of the carbon composite membrane has been visually observed using a scanning electron microscope Joel-JSM, Model 840 A, Japan at 3-keV acceleration voltage. All the membrane samples are dipped in liquid nitrogen and coated with gold to a thickness of ~150 Å, before being analyzed. SEM pictures of both the top surface of the clay support and the carbon membrane are obtained at the magnification of 5 and 10 K, respectively.

Molecular Weight Cutoff. The MWCO of the membrane is defined as the molecular weight of the solute going 90% rejection and is evaluated by analyzing the rejection of 1000 ppm solution of PEG of different molecular weights (200–2500 Da). All the experiments are conducted at room temperature and the membranes are compacted at a pressure (482 kPa) higher than the operating pressure (275.7 kPa) for 5 h before any measurement. The concentration of PEG in the feed and permeate is estimated using refractive index (RI) measurements. The pore diameter of the membrane is determined using the following equation[35]

$$a = 16.73 \times 10^{-10} M^{0.557} \tag{1}$$

where, a is the pore radius of the membrane in cm and M is the molecular weight cut-off of the membrane.

Contact Angle Measurement. To evaluate the hydrophobicity of the membrane surface, the static contact angle of water with the membrane samples has been measured using Goniometer (Model 100-00-230) supplied by ŕame-hart using RH1 2001 Imaging software. Droplets of double distilled water (≈3 ml) were positioned at different places and at least 20 readings were taken to determine the average values.

Membrane Permeability. Pure water flux has been obtained using a lab scale ultrafiltration batch cell as shown in Figure 1. The hydraulic permeability (L_p) of the membrane is determined from the slope of the experimental data for the filtrate flux as a function of the pressure applied.

$$L_p = \frac{J_w}{\Delta P} \tag{2}$$

Before obtaining the water flux the membranes are soaked in water for sometime and compacted with double distilled water at a higher pressure (482 kPa) than the maximum operating pressure till a constant water flux is obtained.

Ultrafiltration Experiments and Analysis

Ultrafiltration experiments have been carried out in dead end type laboratory test cells each having an effective filtration area of 40 cm^2. The batch cell (Figure 1) consists of two parts, cylindrical top part and a base plate made of stainless steel SS316 having a height of 240 mm and an outer diameter of 76 mm. The base plate has circular grooves of 4-mm depth, which houses the membrane. The composite carbon membrane, cast in a perforated stainless steel casing of 60-mm inner diameter and 2–3-mm deep sealed with a fast-setting epoxy resin membrane resin, is placed inside the cylindrical groove of the base plate. The upper half of the cell is fixed to the base plate by nut and bolt and an o-ring is kept on the membrane thus making the

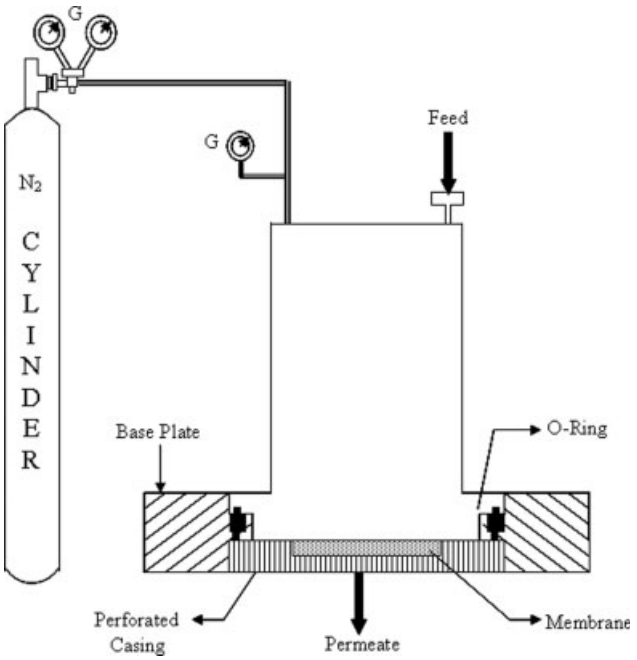

Figure 1. The schematic representation of the unstirred batch ultrafiltration experimental setup where G represents the pressure gauge.

entire setup leak proof. The membrane cross-sectional area available for flux and retention measurements is 28 cm^2.

The membrane is compacted with double distilled water at a higher pressure (482 kPa) than the maximum operating pressure till a constant water flux is obtained. Pure water flux and permeate flux have been obtained by measuring the time required to collect 25 ml permeate volume. For each run, the cell is filled with 500 ml of dye feed solution and permeate flux is measured after 50 ml of permeate passed through the membrane. After each separation experiment, the membrane is cleaned with distilled water at higher pressure (482 kPa) and water flux is determined to ensure that there is no flux decline due to partial plugging.

Ultrafiltration experiments are performed using Acid Orange 7 dye solution and the solute concentration is measured using a UV spectrophotometer (Elico) at 484.5 nm. The separation experiments have been conducted at five different pressures (68–300 kPa) and four different initial concentrations of dye (VI) (10–1000 ppm). Acid Orange 7 has the molecular formula of 4-(2-hydroxy-1-naphthylazo) benzene sulfonic acid sodium salt, having a chemical structure shown in Figure 2 and is an azo dye having an overall negative charge.

In ultrafiltration experiments, the rejection factor is defined as

$$R_{obs}(\%) = \left(1 - \frac{c_p}{c_R}\right) \times 100 \tag{3}$$

$$R_{real}(\%) = \left(1 - \frac{c_P}{c_m}\right) \times 100 \tag{4}$$

where c_p is the solute concentration in permeate, c_R is the solute concentration in retentate (in bulk), c_m is the solute concentration at the membrane interface, R_{obs} is the observed rejection factor, R_{real} is the real or intrinsic rejection factor.

R_{real} is an inherent property of the membrane while R_{obs} depends strongly on the operating conditions and therefore, it is desirable to report separation performance of a membrane in terms of R_{real} even though the determination of c_m is difficult. The membrane surface concentration, c_m, can be determined either directly through interoferometric[36,37] and optical shadow measurements[38,39] or by solving transport equations in the polarization layer. Accuracy of the estimated c_m depends upon the validity of the hydrodynamic model used. In this work, we have determined c_m using the osmotic pressure model[37]

$$J_v = L_p(\Delta P - \sigma\Delta\pi) \tag{5}$$

where J_v is the permeate flux, ΔP, the applied pressure difference, σ, the membrane reflection coefficient and $\Delta\pi$, the osmotic pressure difference. The osmotic pressure difference is calculated using the van't Hoff equation for electrolytes.

$$\Delta\pi = \upsilon RT\Delta C \tag{6}$$

The reflection coefficient is related to the intrinsic rejection of the membrane through the equation given by Spiegler and Kedem.[40]

$$R_{real} = \sigma(1 - F)/(1 - \sigma F) \tag{7}$$

where F is given by

$$F = \exp\{-(1 - \sigma)J_v/P_m\} \tag{8}$$

The c_m, σ, and P_m (solute permeability) are calculated using Eqs. 5–8 following the iterative technique given by Ghose et al.,[41] with the convergence criterion being a change of less than 2% in the value of surface concentration of the membrane (c_m).

Results and Discussion

Preparation of Carbon Membrane

In this work, we have prepared a ceramic supported carbon membrane using a blend of resole type phenol-formaldehyde resin (prepared by condensation polymerization) and PEG of molecular weight 400 Da. The phenolic resins are condensation products of phenol and formaldehyde. The low molecular weight (300–700 g/gmol)[42] resole-type PF (Phenol/formaldehyde = 1.5) resin is formed in presence of basic catalyst (sodium hydroxide) and as the reaction continues,

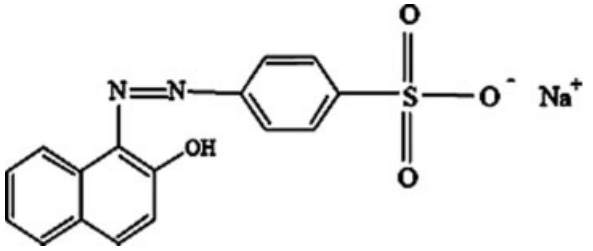

Figure 2. Chemical structure of the dyes Acid Orange 7.

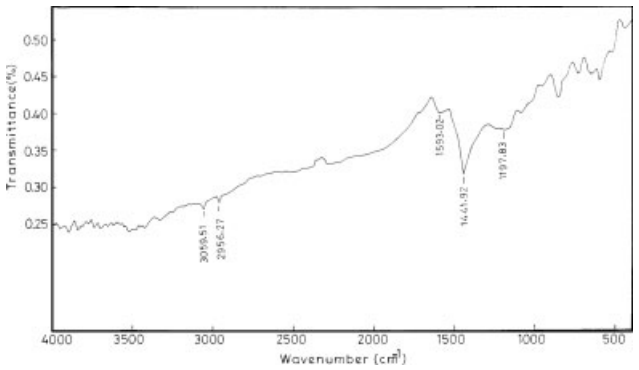

Figure 3. FTIR Spectrum of the carbon membrane.

methylol phenols condense to form methylene bridges to give liquid resols. When such products with ether linkages are heated, they lose 1 mole of formaldehyde between them to form a cross-linked polymer structure.

The polymer blend (PF/PEG) in ethanol is coated on the microporous support which is soaked in xylene, cross-linked and carbonized at 500°C. Here, the PEG acts as the labile phase and the phenol-formaldehyde resin acts as the stable phase. Xylene prevents the polymer to seep inside the pores of the support and the carbon layer lies strictly on the membrane surface (as can also be seen in SEM pictures). During the carbonization process, the evolution of gases reduces the polymer mass on the support leaving behind the solid carbon film. The weight of carbon deposited on the support after two coats of polymer and carbonization has been found to be nearly 45 mg. The PEG is expected to form very little residual carbon as it degrades at a temperature much lower than the carbonization temperature. Thus, PEG acts as a template to pore formation in the carbon membrane and leads to an increase in the permeability and the selectivity of the membrane.

Characterization of the Carbon Membrane

Fourier Transform Infrared Analysis. The FTIR spectrum of the carbon membrane is shown in Figure 3. It can be seen that the bending vibrations appear at 1197 cm^{-1} due to the presence of acid (—COOH), ether, and ester groups, at 1441 cm^{-1} due aliphatic C—H and at 1593 cm^{-1} for aromatic —CH. The stretching vibrations occur at 2956 and 3059 cm^{-1} for the aliphatic and aromatic —CH, respectively.

Scanning Electro Microscopy. The top view of the microporous clay support and the composite membrane are shown in Figures 4a,b. The pores formed in the membrane due to the evolution of gases and PEG decomposition during carbonization are clearly visible in Figure 4b. In this work, the technique of composite membrane preparation is unique as the carbon film lies strictly on the surface and does not penetrate inside the microporous clay support as shown in Figure 4c. This is because, during film casting, the support is completely soaked in a nonsolvent, xylene, which does not allow the polymer to penetrate inside due to the thermodynamic barrier and the film lies on the surface of the support. Moreover, the carbon film formed at the carbonization step is adhering completely to the clay support, maintaining the integrity and the mechanical stability of the composite membrane. The thickness of the carbon membrane has been determined to be 30 μm from the SEM measurements.

Molecular Weight Cutoff Experiments. The molecular weight cut for the carbon membrane (determined by 90% cutoff line) as shown in Figure 5, has been determined to be 1250 Dalton that corresponds to average pore diameters of 1.8 nm (calculated from Eq. 1). This establishes the fact that the membrane prepared is nanoporous and using an additive like PEG makes the membrane more selective to the solutes of low molecular weight.

Contact Angle Measurement. Contact angle with water is a common measure of the hydrophobicity of a surface. Contact angle measurement with water has been found to be 60° showing that the surface of the membrane is hydrophobic as expected for a carbon material.

Membrane Permeability

Experimental data for the permeability of water has been obtained for the carbon membranes as shown in Figure 6. The pure water flux varies linearly (with origin as part of the line) with pressure drop in accordance with the Darcy's law. From the slope of the plot, we have determined the pure water permeability to be 2.09×10^{-7} m/s/kPa (75.35 l/m^2h bar) which is 1.8 times higher than the carbon membrane reported in literature[19] having the maximum permeability 41 l/m^2h bar. This could be attributed to the increase in porosity due to the gas evolving during its formation and decomposition of porogen. The hydraulic permeability obtained for the carbon membrane synthesized in this work is almost two orders of magnitude more that that reported in our earlier work (0.46 l/m^2h bar for the unmodified membrane, 0.60 l/m^2h bar for the nitrated membrane and 0.72 l/m^2h bar for the aminated membrane).[23]

Permeate Flux and Rejection

Effect of Pressure. The membrane so prepared has been used for the separation of Acid Orange 7 dye from its water solution and the permeate flux obtained from the membrane as a function of pressure at different concentrations (10, 50, 100, and 1000 ppm) of the dyes and the results are shown in Figure 7. It can be seen that with the increase in applied pressure, the permeate flux increases linearly. It has been shown that concentration polarization depends upon dimensionless filtration number and higher values of this, a cake layer would form.[43,44] In view of this, after every experimental run, the pure water flux is measured after washing to ensure that there is no flux decline due to formation of a cake.

The rejection of Acid Orange 7 dye as a function of pressure drop at a feed concentration of 10 ppm obtained from the carbon membrane is shown in Figure 8. Since the permeate flux is found to be lower than the pure water flux, this implies that the rejection results have to be corrected to include concentration polarization effects. Thus, the real rejection has been calculated following the procedure developed in the "Ultrafiltration Experiments and Analysis" section to characterize the membrane performance. The concentration of the dye at the surface of the membrane (c_m) is

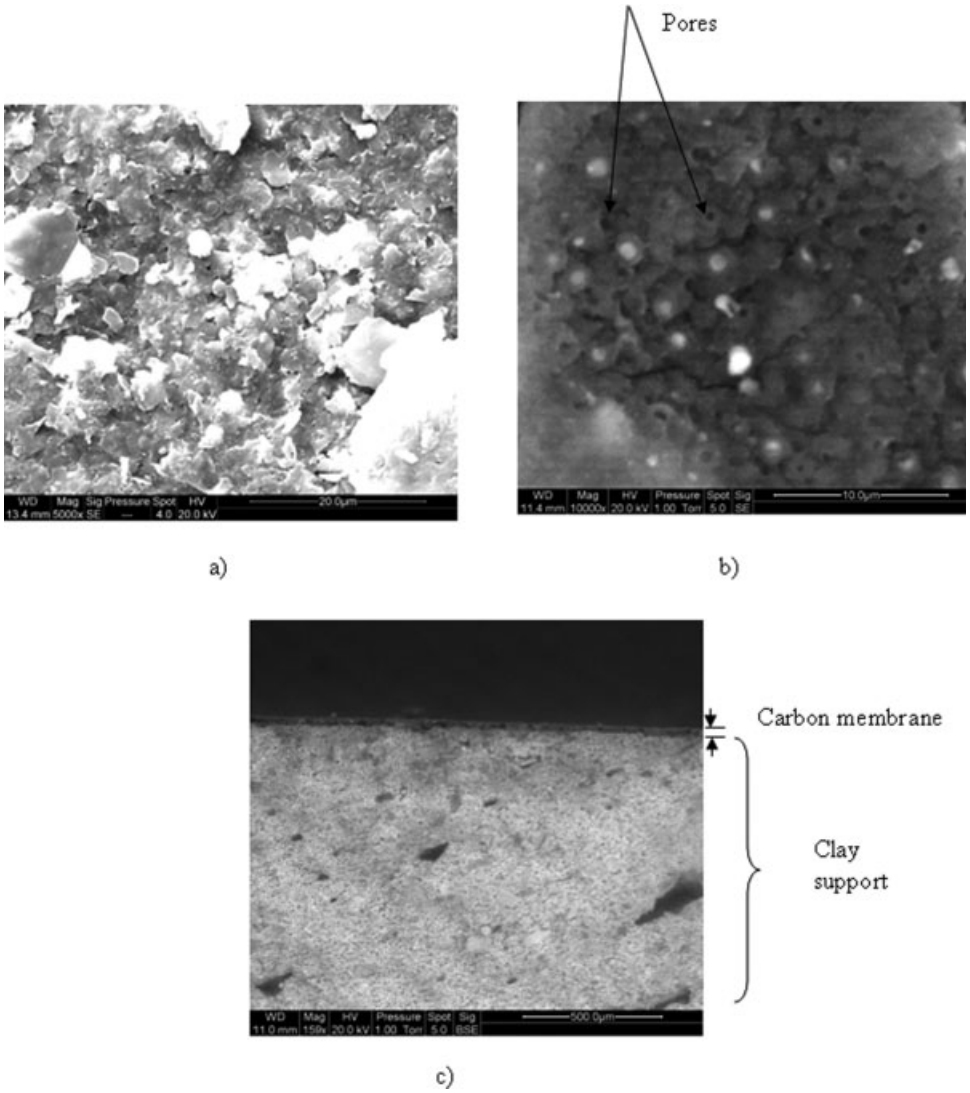

Figure 4. (a) SEM picture of clay support showing macro pores on its surface; (b) porous carbon membrane; (c) cross-sectional view of the membrane.

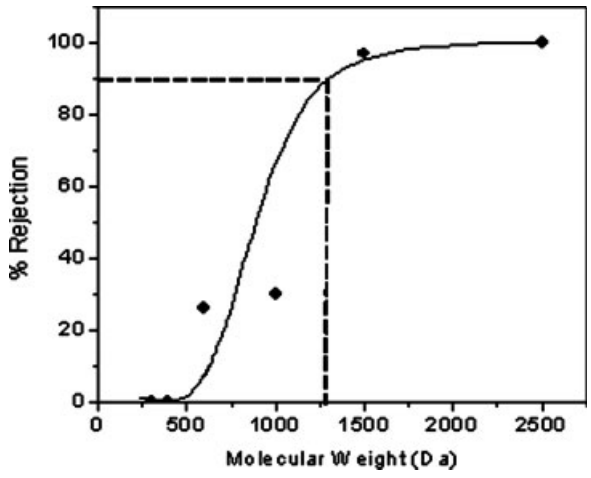

Figure 5. Molecular weight cut off (MWCO) of carbon membrane found to 1250 Da corresponding to a pore diameter of 1.8 nm.

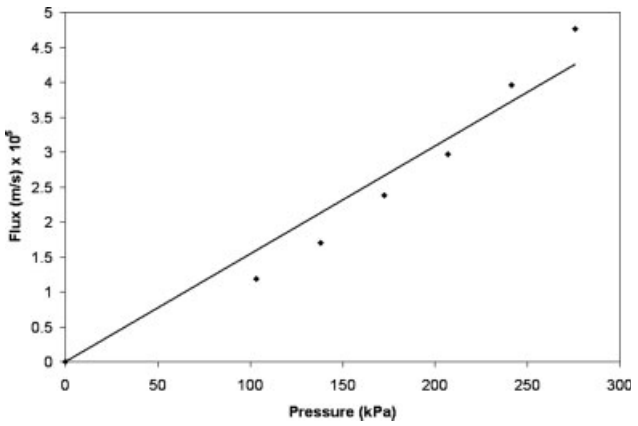

Figure 6. Pure water flux of carbon membrane obtained from the carbon membrane.

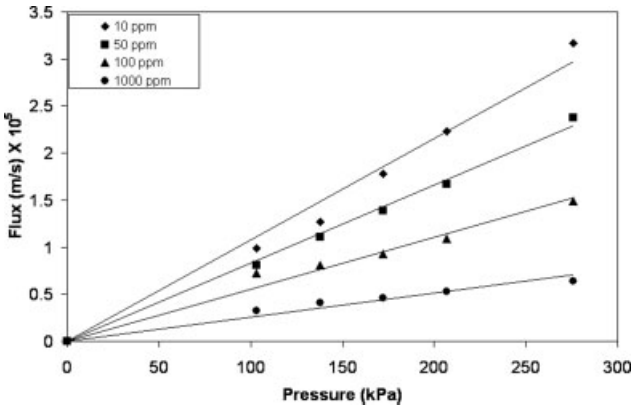

Figure 7. Permeate Flux obtained for different concentrations of Acid Orange 7 dye obtained from the carbon membrane.

determined indirectly using Speigler-Kedam model. It is found that the dye concentration on the membrane surface was 4–5 times higher than the concentration in the bulk. Also, the real rejection of the dyes always increased with pressure, though slightly, due to interaction of ionic solutes with charged membranes.

The MWCO of the carbon membranes (1250 Da) is larger than the molecular weight of the dye molecules (350 Da) to be separated. Therefore, the separation of the dyes must have been affected by the electrostatic interaction of the dyes with the membrane. The carbon membrane after carbonization, is expected to have acid functional groups (COOH) on its surface (can be seen in FTIR spectrum), which should impart a negative charge to it. This explains the rejection of the negatively charged Acid Orange 7 dye (due to Donnan potential). Moreover, in the presence of charged solutes like Acid Orange 7 dye, the membrane can also acquire additional charge.

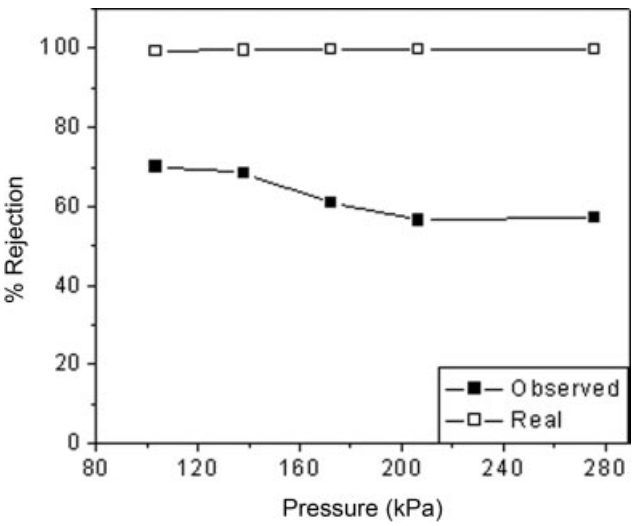

Figure 8. Effect of pressure on observed and real rejection of Acid Orange 7 dye at the feed concentration of 10 ppm obtained from the carbon membrane.

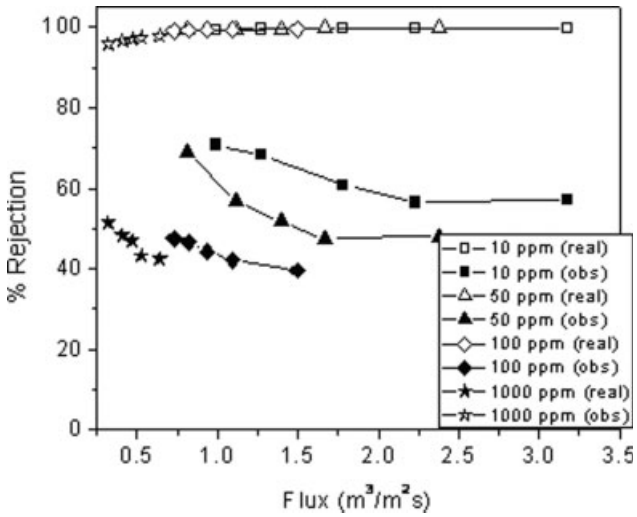

Figure 9. Effect of concentration acid on observed and real rejection of Acid Orange 7 dye obtained from the carbon membrane.

Effect of Feed Concentration. The permeate flux of the dyes have been obtained for different feed concentrations of the solute as shown in Figure 7. As is evident from the figure, the permeate flux for low concentrations (10 ppm), the dye solution is higher as compared to the 50, 100, and 1000 ppm permeate flux. This shows that at higher concentrations, dimensionless filtration number[43,44] is high, this way promoting cake formation near surface and the permeate flow rate therefore decreased with increase in concentration of the dyes. Rejection data of the dye solutions at different feed concentrations has been obtained and experiments have been conducted for the concentration of 10, 50, 100, and 1000 ppm for the carbon membrane as shown in Figure 9. It has been found that the observed rejection of the Acid Orange 7 always increased with the decrease in feed concentration due to the charged nature of the membrane causing the rejection due to Donnan potential.

Analysis Using Space Charge Model

Charged porous membranes have a charge distributed on the surface as well as inside the pores and cannot be measured directly. When an electrolyte comes in contact with a charged membrane pore, an electrical double layer develops within it giving rise to a radial variation of the electrical potential and an unequal distribution of the cations and anions. This results in the development of a nonzero space charge region causing a coupling of electrical forces, mass transfer and fluid flow. Therefore, an estimation of the effective wall potential which characterizes a charged membrane is of great importance. In the model, the membrane is assumed to consist of a collection of long, narrow, parallel cylindrical capillaries carrying a uniformly distributed electrical surface charge. The length of the pores, l, is relatively large as compared to the radius, a ($l \gg a$) as shown in Figure 10a (a schematic of a single capillary). The electrolyte concentrations in the feed and permeate solutions i.e. at either end of the pore are denoted as c_b (upstream

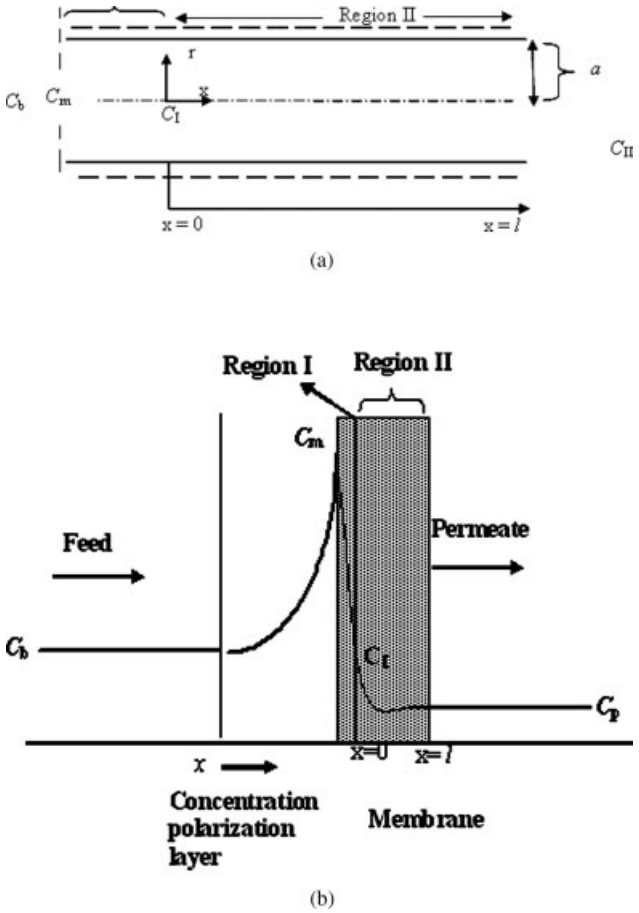

Figure 10. (a) The representation of a negatively charged cylindrical pore in the ultrafiltration membrane; (b) schematic view of the membrane showing the concentration profile of the solute in the bulk, concentration polarization layer and membrane.

concentration) and c_p (downstream concentration), respectively, as shown in Figure 10a. We use cylindrical co-ordinate system (r, θ, x) with x being positive in the direction of decreasing solute concentration. It is further assumed that the ion concentrations and electrical potentials are invariant in θ-direction of the pores.

In our model, we have assumed the membrane capillary to be divided into two regions. In the first region (Region I), decrease in concentration occurs from c_m to c_I due to the unstirred concentration polarization layer (Figure 10b). The value of the c_m is the same as that calculated in the ''Effect of Pressure'' section. The Region II corresponds to the part of the membrane capillaries where the SCM holds well and describes the effect of wall potential on the movement of ions. The concentrations at $x = 0$ mouth and tail of the pore are c_I and c_{II} respectively, and c_{II} is taken to be equal to c_p.

The basic governing equations describing the flow of dye solution through the pore (momentum, convective-diffusion and Poisson-Boltzman equations) are presented in Appendix. The SCM uses Nernst-Planck equation (Eq. A1 of appendix) to determine the flux of ions, Navier-Stokes equation (Eq. A2 of appendix) to determine the fluid dynamics (bulk velocity/volume flow) and Poisson-Boltzmann equation (Eq. A4 of appendix) to relate the distribution of electrical potential to the space charge density (concentration profile of solutes). It may be noticed that the system of governing equation represents a set of coupled nonlinear differential equation and they have to be solved simultaneously. All the equations are written in nondimensionalized form and for the nondimensionalization of concentration, c_I and solute flux J_s, we have taken the permeate concentration (c_{II}) instead of the upstream concentration (c_I), as done by Sasidhar and Ruckenstein[32]). On doing this, it can be easily seen that the ratio J_s^*/Pe is equal to 1, which leads to incorporation of the concentration polarization effects in a natural way and also simplifies the computation scheme. The Poisson-Boltzman equation has been solved using a series solution already discussed in our previous work.[33] The experimental data (Pe_p^{exp} and Pe^{exp}) are fitted to calculate the concentration at the interface of the membrane (including the rise in bulk concentration due concentration polarization) and the wall potential which are difficult to measure directly.

The physical data that the model uses includes diffusion coefficients of the ions (D_i), Faraday's constant (F), universal gas constant ($\Re$), temperature (T), dielectric constant (ε_0) and dynamic viscosity of the water (μ). It is known that in confined pores molecules diffuse much slower compared to that in bulk water. In this work, due to lack of experimental data, as a first approximation, we have assumed this to be the same as in bulk, and in view of this, the surface charges estimated using space charge model are likely to be on higher side. The bulk diffusion coefficient values in water are used in this study and are determined from the data of equivalent conductance of ions at infinite dilution as given in the literature.[45] In addition to these, the model requires characteristic membrane structural parameters like pore diameter, membrane area and pore length which are experimentally known to be 1.8 nm, 28 cm^2, and 30 μm (measured from SEM picture Figure 4c), respectively, for fitting of the experimental results. In order to check the efficiency of our numerical procedure, we have performed the simulation on Pentium IV PC using MATLAB 7.1 software. The tolerance value for the numerical calculation of the solution of Poisson-Boltzmann equation was kept at 10^{-6}. The analysis presented in this work determines the wall potential of this region (region II) and the concentration at $x = 0$ (c_I) in Figures 10a, b which would give the experimentally measured flux. To show that the series solution reduces the computational load drastically, the CPU time required was determined as a function of wall potential and λ. For a typical simulation with the same initial values of pore size and wall potential, the time taken for series solution method is about 15 min as compared to 15 h taken by MATLAB 7.1 solver for ordinary differential equation for the complete numerical integration.

Using the SCM, the wall potential of the carbon membranes was calculated corresponding to each pressure at which the experimental data was obtained. The carbon membrane has acid functional groups on its surface imparting a negative charge which is responsible for the separation of Acid Orange dyes and we have obtained the wall potentials presented in Table 1 based on the experimental results of Acid Orange dye. The wall potentials have been obtained,

Table 1. Wall Potential Obtained for the Separation of Acid Orange 7 Dye for Different Concentrations of the Dye

Applied Pressure (kPa)	Value of Charge (mV)			
	Dye Concentration (ppm)			
	10	50	100	1000
103.4	−102.7	−102.7	−96.79	−96.79
137.9	−102.7	−99.1	−96.54	−88.83
172.4	−100.39	−97.82	−96.02	−88.58
206.8	−98.85	−97.05	−95.77	−88.06
275.8	−98.85	−96.79	−95.51	−87.29

for each value of the dye concentration as a function of pressure. The potential varies in the range from −100 to −85 mV decreasing with the increasing concentration, showing an effect of depolarization with the increase in dye concentration. This is similar to the trend obtained from the separation data using charged membranes.

Conclusion

A composite nanoporous (pore size 1.8 nm as determined from the molecular weight cutoff experiments) carbon membrane has been synthesized using a polymer blend of polyethylene glycol (400 Da) and phenol formaldehyde resin. The membrane obtained has a higher water permeability compared to those reported in literature. The separation of the dye solution by the carbon membrane has been modeled by Space charge model in which the latter was assumed to consist of capillaries of diameter 1.8 nm and the length of 30 μm (equal to the thickness of the membrane). It has acid functional groups (confirmed by the FTIR) on its inner surface which impart negative charge to it making it possible to separate negatively charged Acid Orange 7 dye. The effect of pressure and feed concentration on dye rejection has been studied and it was found that the real rejection increased with increase in the pressure and decreased with concentration. The separation results have analyzed using Space charge model and the effective wall potential of the membrane has been determined to be varying in the range of −100 to −85 mV in the range of feed concentration studied.

Notation

a = pore radius, m
l = length of pore, m
A = area of the cross section of the pore, m^2
c = concentration of the electrolyte, moles/m^3
c_I = concentration in the polarization layer, moles/m^3
c_p = concentration in the permeate, moles/m^3
$\bar{c}$ = dimensionless concentration of the electrolyte, c/c_{II}
D_i = diffusion coefficient of the ith ion, m^2/s
d = ratio of diffusion coefficients
F = Faradays constant, Coulomb/mole
$j_{i,x}$ = flux of the ith ion in the axial direction, moles/m^2/s
$j_{i,r}$ = flux of the ith ion in the radial direction, moles/m^2/s
J = total solute flux rate across the pore, moles/s
J_w = pure water flux, m/s
J_s = average solute flux across the pore, moles/s
J_s^* = dimensionless solute flux
k_i = the integral defines by Table A1.
L_i = coefficients defined by Eq. A8.
P = pressure, N/m^2
Pe = Peclet number: dimensionless average velocity through the pore
Pe_p = pressure Peclet number
Pe_π = osmotic pressure Peclet number
R = gas constant
T = absolute Temperature, K
U = average velocity, m/s
u_x = axial velocity, m/s
u_r = radial velocity, m/s
Q = volumetric flow rate, m^3/s
Y = dimensionless solvent pressure
z_i = valency of the ith ion
R_m = intrinsic hydraulic resistance
L_p = hydraulic permeability

Greek letters

ε = dielectric constant
μ = viscosity of the medium, Poise
μ_w = viscosity of water, Poise
λ_D = Debye length, cm
σ = surface charge density of the pores of the wall, C/m^2
ξ = dimensionless axial position, x/l
ω = dimensionless parameter defined by $4a^2RTc(x)/\mu D_+$
λ = dimensionless Debye length, λ_D/a
Φ = total electrostatic potential, V
ϕ = axial component of potential, V
$\bar{\phi}$ = dimensionless potential, $F\phi/RT$
ψ = electric potential due to double layer, V
$\bar{\psi}$ = dimensionless double layer potential, $F\psi/RT$
Ψ_w = wall potential

Subscripts

I, II = denotes two regions
i = denotes the ith ion; +, cation and −, anion
s = solute
w = wall

Literature Cited

1. Keizer K, Verweij H. Progress in inorganic membranes. *Chemtech*. 1996;26:37–41.
2. Zaman J, Chakma A. Inorganic membrane reactors. *J Membr Sci*. 1994;92:1–28.
3. Ismail AF, David LIB. A review on the latest development of carbon membranes for gas separation. *J Membr Sci*. 2001;193:1–18.
4. Saufi SM, Ismail AF. Fabrication of carbon membranes for gas separation–a review. *Carbon*. 2004;42:241–259.
5. Koresh JE, Soffer A. The carbon molecular sieve membranes. General properties and the permeability of CH_4/H_2 mixture. *Sep Sci Technol*. 1987;22:973–982.
6. Koresh JE, Soffer A. Mechanism of permeation through molecular-sieve carbon membrane. Part 1: The effect of adsorption and the dependence on pressure. *J Chem Soc Faraday Trans I*. 1986;82:2057–2063.
7. Kawai T, Tatsuo N. Jpn Kokai Tokkyo Koho JP 60179102, 1985.
8. Bromhead J, Clint JH, Lear AM, Oliver LF, Tennison SR. Eur Pat Appi. EPO474424A2, 1991.
9. Chen YD, Yang RT. Preparation of carbon molecular sieve membrane and diffusion of binary mixtures in the membrane. *Ind Eng Chem Res*. 1994;33:3146–3153.
10. Petersen J, Matsuda M, Haraya K. Capillary carbon molecular sieve membranes derived from Kapton for high temperature gas separation. *J Membr Sci*. 1997;131:85–94.
11. Ash R, Barrer RM, Lowson RT. Transport of single gases and of binary gas mixtures in a microporous carbon membrane. *J Chem Soc Faraday Trans I*. 1973;69:2166–2178.
12. Schumacher H, Juntgen H, Preuss E, Zundorf D, Hodek W, Romey I. Membrane with preselected pore types for separation processes. US Patent 4261832, 1981.
13. Liang C, Sha G, Guo S. Carbon membrane for gas separation derived from coal tar pitch. *Carbon*. 1999;37:1391–1397.

14. Song C, Wang T, Pan Y, Qiu J. Preparation of coal-based microfiltration carbon membrane and application in oily wastewater treatment. *Sep Purif Technol*. 2006;51:80–84.
15. Kishore N, Sachan S, Rai KN, Kumar A. Synthesis and characterization of a nanofiltration carbon membrane derived from phenol-formaldehyde resin. *Carbon*. 2003;41:2961–2972.
16. Lee HJ, Suda H, Haraya K, Moon SH. Gas permeation properties of carbon molecular sieving membranes derived from the polymer blend of polyphenylene oxide (PPO)/polyvinylpyrrolidone (PVP). *J Membr Sci*. 2007;296:139–146.
17. Kim YK, Park HB, Lee YM. Carbon molecular sieve membranes derived from thermally labile polymer containing blend polymers and their gas separation properties. *J Membr Sci*. 2004;243:9–17.
18. Strano MS, Zydney AL, Barth H, Wooler G, Agarwal H, Foley H. C. Ultrafiltration membrane synthesis by nanoscale templating of porous carbon. *J Membr Sci*. 2002;198:173–186.
19. Shah TN, Foley HC, Zydney AL. Development and characterization of nanoporous carbon membranes for protein ultrafiltration. *J Membr Sci*. 2007;295:40–49.
20. Pan Y, Wang W, Wang T, Yao P. Fabrication of carbon membrane and microfiltration of oil-in-water emulsion: an investigation on fouling mechanisms. *Sep Purif Technol*. 2007;57:388–393.
21. Wei W, Hu H, Qin G, You L, Chen G. Pore structure control of phenol-formaldehyde based carbon microfiltration membranes. *Carbon*. 2004;42:679–681.
22. Nishiyama N, Dong YR, Zheng T, Egashira Y, Ueyama K. Tertiary amine-mediated synthesis of microporous carbon membranes. *J Membr Sci*. 2006;280:603–609.
23. Pugazhenthi G, Sachan S, Kishore N, Kumar A. Separation of chromium (VI) using modified ultrafiltration charged carbon membrane and its mathematical modeling. *J Membr Sci*. 2005;254:229–239.
24. Santos AB, Cervantes FJ, Lier JB. Review paper on current technologies for decolorization of textile wastewaters: Perspectives for anaerobic biotechnology, *Bioresour Technol*. 2007;98:2369–2385.
25. Meric S, Selcuk H, Gallo M, Belgiorno V. Decolourisation and detoxifying of Remazol Red dye and its mixture using Fenton's reagent. *Desalination*. 2005;173:239–248.
26. Hamada K, Nishizawa M, Yoshida D, Mitsuishi M. Degradation of an azo dye by sodium hypochlorite in aqueous surfactant solutions. *Dyes Pigment*. 1998;36:313–322.
27. Hsing HJ, Chiang PC, Chang EE, Chen M. Y The decolorization and mineralization of Acid Orange 6 azo dye in aqueous solution by advanced oxidation processes: a comparative study. *J Hazard Mater*. 2007;141:8–16.
28. Prieto O, Fermoso J, Nunez Y, del Valle JL, Irusta R. Decolouration of textile dyes in wastewaters by photocatalysis with TiO_2. *Solar Energy*. 2005;79:376–383.
29. Robinson T, McMullan G, Marchant R, Nigam P. Remediation of dyes in textile effluent: a critical review on current treatment technologies with a proposed alternative. *Bioresour Technol*. 2001;77:247–255.
30. Pearce CI, Lloyd JR, Guthrie JT. The removal of color from textile wastewater using whole bacterial cells: a review. *Dyes Pigment*. 2003;58:179–196.
31. Forgacs E, Cserhati T, Oros G. Removal of synthetic dyes from wastewater: a review, *Environ Int*. 2004;30:953–971.
32. Liu H, Li G, Qua J, Liu H. Degradation of azo dye Acid Orange 7 in water by Fe°/granular activated carbon system in the presence of ultrasound. *J Hazard Mater*. 2007;144:180–186.
33. Sasidhar V, Ruckenstein E. Electrolyte osmosis through capillaries. *J Colloid Interface Sci*. 1981;82:439–457.
34. Sachdeva S, Kumar A. Synthesis and modeling of composite poly (styrene-co-acrylonitrile) membrane for the separation of chromic acid. *J Membr Sci*. 2008;307:37–52.
35. Singh S, Khulbe KC, Matsuura T, Ramamurthy P. Membrane characterization by solute transport and atomic force microscopy. *J Membr Sci*. 1998;142:111–127.
36. Mahlab, Yosef NB, Belfort G. Interferometric measurement of concentration polarization profile for dissolved species in unstirred batch hyperfilteration (reverse osmosis). *Chem Eng Commun*. 1980;6:225–243.
37. Clifton M. *Polarization de concentration dans divers procedes de separation a membrane*, These, Universite Paul Sabatier, Toulhouse, France, 1982.
38. Vilker VL, Colton CK, Smith KA, Green DL. Concentration polarization in protein ultrafiltration. Part 1: An optical shadowgraph technique for measuring concentration profiles near a solution-membrane interface. *AIChE J*. 1981;27:632–637.
39. Vilker VL, Colton CK, Smith KA, Green DL. Concentration polarization in protein ultrafiltration. Part 2: Theoretical and experimental studies of albumin ultrafiltered in an unstirred cell. *AIChE J*. 1981;27:637–645.
40. Spiegler KS, Kedem O. Thermodynamics of hyperfiltration (reverse osmosis): criteria for efficient membranes. *Desalination*. 1966;1:311–326.
41. Ghose S, Bhattacharjee C, Datta S. Simulation of unstirred batch ultrafiltration process based on reversible pore-plugging model. *J Membr Sci*. 2000;169:29–38.
42. Sorenson WR, Campbell TW. *Preparative Methods of Polymer Chemistry*, Inter Science Publishers. New York, 1961.
43. Song L, Elimelech M. Theory of concentration polarization in cross-flow filtration. *J Chem Soc Faraday Trans*. 1995;91:3389–3398.
44. Bhattacharjee S, Kim AS, Elimelech M. Concentration Polarization of interacting solute particles in cross-flow membrane filtration. *J Colloid Interface Sci*. 1999;212:81–99.
45. Coury L. Conductance measurements Part 1: Theory. *Curr Sep*. 1999;18:91–96.

Appendix

Physical model and governing equations

Nernst Planck equation giving the ion flux density:

$$\left.\begin{aligned} j_{i,x} &= u_x c_i - D_i \frac{\partial c_i}{\partial x} - \frac{D_i}{\Re T} z_i c_i F \frac{\partial \Phi}{\partial x} \quad \text{(a)} \\ j_{i,r} &= u_r c_i - D_i \frac{\partial c_i}{\partial r} - \frac{D_i}{\Re T} z_i c_i F \frac{\partial \Phi}{\partial r} \quad \text{(b)} \end{aligned}\right\} \tag{A1}$$

Navier-Stokes equation giving the steady state fluid velocity:

$$\left.\begin{aligned} 0 &\cong -\frac{\partial P}{\partial x} - \left(\sum_i F z_i c_i\right)\frac{\partial \Phi}{\partial x} + \mu\left(\frac{1}{r}\frac{\partial}{\partial r}\left(r\frac{\partial u_x}{\partial r}\right) + \frac{\partial^2 u_x}{\partial x^2}\right) \quad \text{(a)} \\ 0 &\cong -\frac{\partial P}{\partial r} - \left(\sum_i F z_i c_i\right)\frac{\partial \Phi}{\partial r} + \mu\left(\frac{1}{r}\frac{\partial}{\partial r}\left(r\frac{\partial u_r}{\partial r}\right) + \frac{\partial^2 u_r}{\partial x^2}\right) \quad \text{(b)} \end{aligned}\right\} \tag{A2}$$

Poisson Boltzmann equation giving the relation between electrical potential and the charge density:

$$\frac{1}{r}\frac{\partial}{\partial r}\left(r\frac{\partial \Phi}{\partial r}\right) + \frac{\partial^2 \Phi}{\partial x^2} = -\frac{\rho}{\varepsilon} = -\frac{F}{\varepsilon}\sum_i c_i \tag{A3}$$

$$\frac{1}{\eta}\frac{\partial}{\partial \eta}\left(\eta\frac{\partial \bar{\psi}}{\partial \eta}\right) = \frac{1}{\lambda^2}\sinh(\bar{\psi}) \tag{A4}$$

where,

$$\bar{\psi} = \frac{F\psi}{\Re T}, \eta = \frac{r}{a} \text{ and } \lambda = \frac{\kappa}{a}, \quad \kappa = \left(\frac{\varepsilon \Re T}{2F^2 c(x)}\right)$$

The boundary conditions

$$\left.\begin{aligned} &\left.\frac{\partial\bar{\psi}}{\partial\eta}\right|_{\eta=0} = 0 && \text{(a)}\\ &\bar{\psi}\big|_{\eta=1} = \bar{\psi}_{\mathrm{w}} \quad \text{or,} && \text{(b)}\\ &\left.\frac{\partial\bar{\psi}}{\partial\eta}\right|_{\eta=1} = \bar{q} = \frac{Fqa}{\varepsilon RT} && \text{(c)} \end{aligned}\right\} \tag{A5}$$

Since, there is no current flow, the governing equations can be written in dimensionless form as:

$$Pe \triangleq \frac{Ul}{D_+} = -\frac{L_3}{\bar{c}}\frac{d\bar{c}}{d\xi} + L_4\frac{dY}{d\xi} \tag{A6}$$

$$J_s^* = -L_1\frac{d\bar{c}}{d\xi} + \bar{c}L_2\frac{dY}{d\xi} \tag{A7}$$

where

$$\xi = \frac{x}{l},\ \bar{c} = \frac{c(x)}{c_{II}},\ \bar{\phi} = \frac{F\phi}{RT},\ \omega = \frac{4a^2RTc(x)}{\mu D_+}$$

$$Y = -\frac{a^2}{8\mu D_+}(P-\pi), J_s^* = \frac{J_s l}{D_+ c_{II}}$$

$$\left.\begin{aligned} L_1 &= k_5 + \omega k_7 - \frac{(k_4-\omega\lambda^2k_8)(k_4+\omega k_3)}{(k_5-\omega\lambda^2k_6)} && \text{(a)}\\ L_2 &= 4k_9 - 4k_2\frac{(k_4-\omega\lambda^2k_8)}{(k_5-\omega\lambda^2k_6)} && \text{(b)}\\ L_3 &= \omega k_1 - \omega\lambda^2k_0\frac{(k_4+\omega k_3)}{(k_5-\omega\lambda^2k_6)} && \text{(c)}\\ \text{and}\quad L_4 &= 1 + \frac{4\omega\lambda^2k_0k_2}{(k_5-\omega\lambda^2k_6)} && \text{(d)} \end{aligned}\right\} \tag{A8}$$

The k_i's above are given in Table A1 obtained by using series solution given in reference 33. In terms of L_1 to L_4, Eqs. A6 and A7 are integrated to

$$Pe = \int_{\bar{c}(\xi=0)}^{\bar{c}(\xi=1)} \left\{\frac{L_2L_3 - L_1L_4}{(J_s^*/Pe)L_4 - \bar{c}L_2}\right\} d\bar{c} \tag{A9}$$

$$-\frac{a^2}{8\mu D_+}\Big[(P-\Pi)_{\xi=1} - (P-\Pi)_{\xi=0}\Big] = \int_{\bar{c}(\xi=0)}^{\bar{c}(\xi=1)} \left\{\frac{(J_s^*/Pe)L_3 - \bar{c}L_1}{(J_s^*/Pe)L_4 - \bar{c}L_2}\right\}\frac{d\bar{c}}{\bar{c}} \tag{A10}$$

Manuscript received Feb. 29, 2008, revision received, Oct. 8, 2008.

Table A1. Integral and Analytical Expressions Derived for k_i

Analytical Solution
$k_0 = \sum_{i=0}^{\infty}\frac{ia_i}{2(i+2)}$
$k_1 = \lambda^2\sum_{i=0}^{\infty}\frac{b_i}{2(i+2)(i+4)}$
$k_2 = \sum_{i=0}^{\infty}\frac{2(i+2)a_{i+2}}{i+4}$
$k_3 = \lambda^2\sum_{i=0}^{\infty}\frac{b_i}{(i+2)^2}\sum_{i=0}^{\infty}(i+2)^2a_{i+2} - \sum_{i=0}^{\infty}\sum_{j=0}^{i}\frac{(i+2-j)^2a_{i+2-j}b_j}{(i+4)(j+2)^2}$
$k_4 = \lambda^2(d+1)\sum_{i=0}^{\infty}(i+2)a_{i+2} + \lambda^2(d-1)\sum_{i=0}^{\infty}\frac{b_i}{(i+2)}$
$k_5 = \lambda^2(d-1)\sum_{i=0}^{\infty}(i+2)a_{i+2} + \lambda^2(d+1)\sum_{i=0}^{\infty}\frac{b_i}{(i+2)}$
$k_6 = \sum_{i=0}^{\infty}\sum_{j=0}^{i}\frac{(i-j+2)^2a_ja_{i-j+2}}{i+2} - \sum_{i=0}^{\infty}a_i\sum_{i=0}^{\infty}(i+2)a_{i+2}$
$k_7 = \lambda^2\sum_{i=0}^{\infty}\sum_{j=0}^{i}\frac{b_jb_{i-j}}{(i+1)^2(i+1)} + \sum_{i=0}^{\infty}\frac{b_i}{(i+2)^2}\sum_{i=0}^{\infty}\frac{b_i}{i+2}$
$k_8 = \lambda^2\sum_{i=0}^{\infty}\sum_{j=0}^{i}\frac{a_jb_{i-j}}{i+2} - \lambda^2\sum_{i=0}^{\infty}a_i\sum_{i=0}^{\infty}\frac{b_i}{i+2}$
$k_9 = \lambda^2\sum_{i=0}^{\infty}\frac{2b_i}{(i+2)(i+4)}$

where $\bar{\psi} = \sum_{i=0}^{\infty}a_i\eta_i$ $\quad \cos h(\psi_{\mathrm{w}}) = \lambda^2\frac{\sum_{i=0}^{\infty}(i+1)(i+3)^2a_{i+3}\eta^i}{\sum_{i=0}^{\infty}(i+3)a_{i+1}\eta^i} = \lambda^2\sum b_i\eta^i$

$$\sin h\,\bar{\psi} = \lambda^2\sum_{i=0}^{\infty}(i+2)^2a_{i+2}\eta^i$$